



CHORUS

This is the accepted manuscript made available via CHORUS. The article has been published as:

Visualizing Mie Resonances in Low-Index Dielectric Nanoparticles

Jing Zhou, Ashwin Panday, Yuntao Xu, Xi Chen, Long Chen, Chengang Ji, and L. Jay Guo

Phys. Rev. Lett. **120**, 253902 — Published 18 June 2018

DOI: [10.1103/PhysRevLett.120.253902](https://doi.org/10.1103/PhysRevLett.120.253902)

1 Visualizing Mie resonances in low-index 2 dielectric nanoparticles

3 *Jing Zhou^{1,2}, Ashwin Panday³, Yuntao Xu¹, Xi Chen⁴, Long Chen⁴, Chengang Ji¹,*

4 *L. Jay Guo^{1,3,4*}*

5 ¹Department of Electrical Engineering and Computer Science, The University of
6 Michigan, Ann Arbor, Michigan 48109, USA.

7 ² State Key Laboratory of Infrared Physics, Shanghai Institute of Technical Physics,
8 Chinese Academy of Sciences, 500 Yutian Road , Shanghai 200083 , China

9 ³Macromolecular Science and Engineering, The University of Michigan, Ann Arbor,
10 Michigan 48109, USA.

11 ⁴Applied Physics, The University of Michigan, Ann Arbor, Michigan 48109, USA.

12 **KEYWORDS:** Nanoparticles, low refractive index, optical nanocavities, visible range

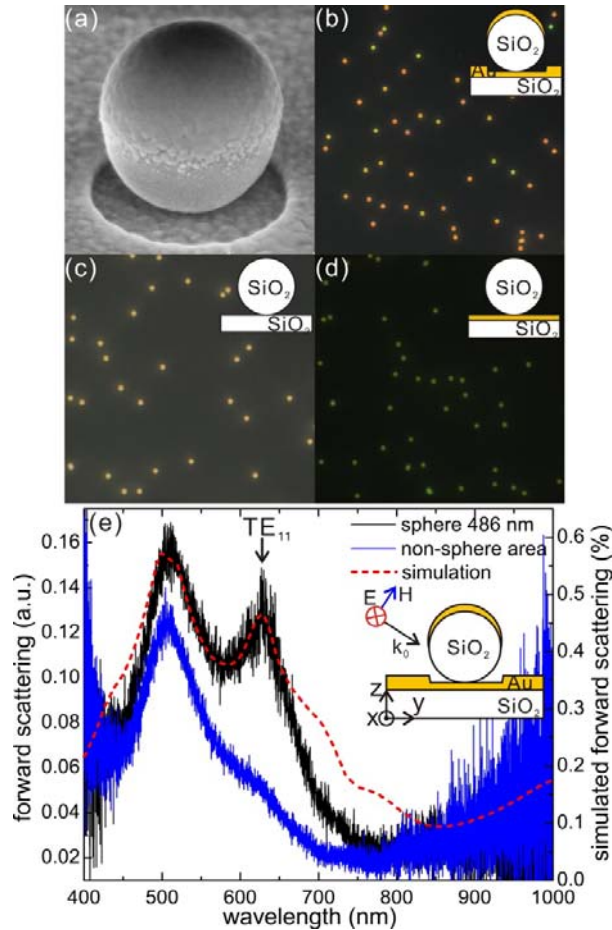
13 **ABSTRACT:** Resonant light scattering by metallic and high-index dielectric
14 nanoparticles has received enormous attention and found many great applications.
15 However, low-index dielectric nanoparticles typically do not show resonant scattering
16 behaviors due to poor light confinement caused by small index contrast. This letter
17 describes a simple and effective approach to drastically enhance the resonance effect
18 of the low-index particles by partial metal dressing. Mie resonances of low-index
19 nanoparticles can now be easily visualized by scattered light. This scattering peak
20 depends on sphere size and has a reasonable line width. A size difference as small as
21 8 nm was resolved by peak shift or even by color change. The scattering peak is
22 attributed to the enhanced TE₁₁ Mie resonance of the low-index nanospheres. The
23 metal dress not only provides high-reflection boundary, but also functions as an
24 antenna to couple the confined light power to the far field, leading to scattering
25 maxima in the spectra. Additionally, the enhanced TE₁₁ Mie resonance in low-index
26 nanoparticles features considerable magnetic response due to the strong circulating
27 displacement currents induced by the intensified *E*-field instead of a high permittivity
28 for index particles. The enhanced Mie resonances could be used to sense minute
29 changes in size or refractive index of low-index nanoparticles and benefit a wide
30 range of applications.

31 TEXT:

32 Light scattering by small particles is a fundamental topic in electromagnetics and
33 attracts much attention throughout modern history [1]. Among all the phenomena,
34 resonant scattering is the most outstanding behavior because it can be easily detected
35 by spectroscopy and features a strong local field, enabling various applications of
36 nanoparticles [2-8]. Metallic nanoparticles with localized surface plasmon resonances
37 have been extensively studied and practically utilized in surface enhanced
38 spectroscopy and metamaterials [9-11]. Recently, high-index dielectric nanoparticles
39 with strong Mie resonances drew considerable interest. Efficient field localization and
40 negligible material absorption facilitate prominent Mie resonances, leading to optical
41 magnetic response and scattering manipulation [7,8,12-16]. For low-index dielectric
42 nanoparticles, the Mie resonances are weak and broad due to poor light confinement
43 caused by low reflection at particle boundaries, so that they are typically not visible in
44 light scattering spectra. However, low-index dielectric nanoparticles, such as SiO₂ and
45 polystyrene nanoparticles, have more applications than their high-index or even
46 metallic counterparts. If pronounced Mie resonances can be realized, many potential
47 applications can be envisioned. In this work, we introduce a metal dressing approach
48 to enhance Mie resonances of low-index nanoparticles so that they can be easily
49 visualized by scattered light. The metal dress improves light confinement ability of
50 the low-index nanoparticles by enhancing boundary reflection. In addition, the open
51 configuration of the metal dress turns dark modes bright. We experimentally and
52 theoretically investigated the metal-dressed SiO₂ nanospheres. While strong
53 plasmonic resonance associated with the crescent shape structures [17,18] occur in
54 sub-100nm size particles, they become very weak in the NIR range for large particles.
55 In this work, we found significantly enhanced TE₁₁ Mie mode in the visible range.
56 Low order Mie resonances scales almost linearly with the particle size, allowing us to
57 distinguish an 8 nm size difference. At this resonance, the strong circulating
58 displacement currents induced by the intensified *E*-field rather than high permittivity
59 could result in considerable magnetic response. The enhanced Mie resonances could
60 be used to sense minute changes in size or refractive index and thus benefit a lot of

61 applications utilizing the low-index nanoparticles.

62 The metal-dressed SiO₂ nanospheres were created by a two-step metal deposition
63 process by electron beam evaporation. First, a thin metal film was deposited on a
64 transparent glass substrate. Then, a dilute solution of nanospheres was spin-casted on
65 the metal film to create well-separated particle distribution. Finally, another thin metal
66 film was deposited on top of the particle and also on the first metal layer. With this
67 process, each of the SiO₂ nanospheres is partially covered by a metal cap and located
68 in a shallow well in the metal film (Fig. 1(a)). In our case, the substrate is fused silica
69 and the deposited metal films are both Au, each with 30 nm thickness. According to
70 SEM inspection, the sizes of the SiO₂ nanospheres range from 400 nm to 500 nm. In
71 the microscopic dark field transmission view, the metal-dressed nanospheres exhibit
72 different colors (Fig. 1(b)). The NA of the dark field condenser is 0.80-0.95 and that
73 of the objective is 0.75. In comparison, bare SiO₂ nanospheres could be identified (Fig.
74 1(c)), but shows no distinct color difference despite slightly different sizes because of
75 their flat scattering spectra. At middle stage of the two-step metal deposition process,
76 where bare SiO₂ nanospheres are located on a thin Au film, there is also no color
77 difference over individual nanospheres (Fig. 1(d)). The greenish color comes from the
78 transmission through Au film that allows a higher transmission of green light.



79

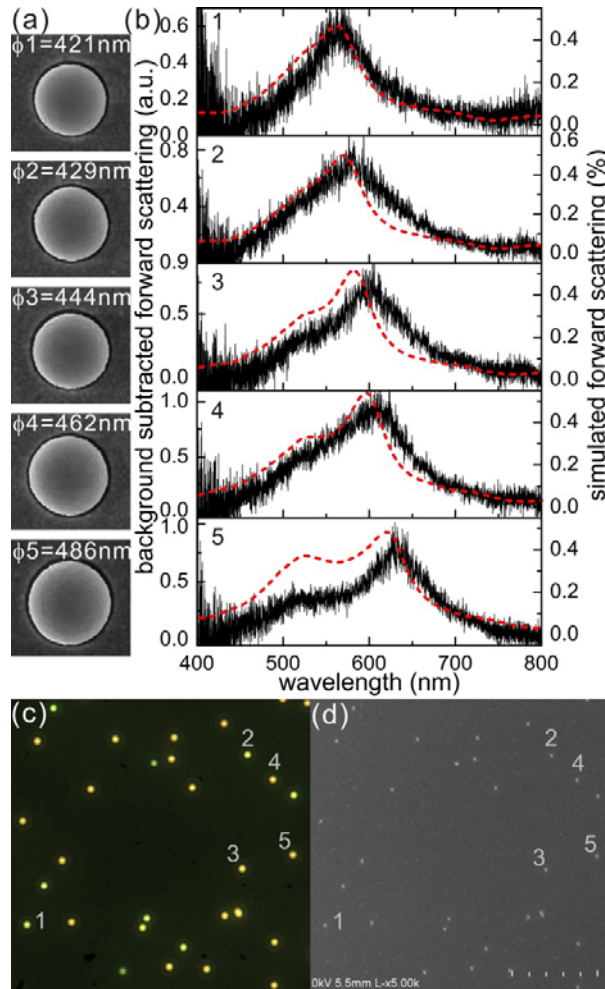
80 Fig. 1 (a) SEM image of a metal-dressed SiO₂ nanosphere. (b)-(d) Microscopic dark
 81 field transmission views of metal-dressed SiO₂ nanospheres, SiO₂ nanospheres on a
 82 fused silica substrate and SiO₂ nanospheres on a 30 nm Au film over a fused silica
 83 substrate. (e) Measured forward scattering spectrum of a 486 nm nanosphere (black)
 84 together with simulation (red), and that at a blank area without nanospheres (blue).
 85 The simulated spectrum is normalized to the incident power. The incident *E*-field is
 86 along the *x*-axis.

87 With a multimode fiber (core diameter ~200 nm), the dark field transmission of a
 88 single nanosphere could be selectively collected and analyzed by a spectrometer.
 89 Since the background transmission is significantly suppressed, the local property of
 90 any single metal-dressed nanosphere could be revealed by the spectrum. For example,
 91 the dark field transmission at a nanosphere with a diameter around 486 nm (size
 92 determined by SEM) is plotted in Fig. 1(e) (black curve). The peak around 510 nm is
 93 due to the interband transition in Au. This can be confirmed by analyzing the stray
 94 light through a blank area without any nanospheres but only the 60 nm Au film; the

95 peak around 510 nm in the spectrum (blue curve in Fig. 1(e)) is attributed to the
96 material property of Au film only. The peak around 630 nm is a resonance of the
97 metal-dressed SiO₂ nanosphere and responsible for the distinctive colors. Simulations
98 by finite element method were also performed for comparison. The forward scattering
99 was simulated by integrating the transmitted power over a solid angle corresponding
100 to the NA of the objective lens. The simulated spectrum (dashed red curve in Fig. 1(e))
101 agrees with the measurement (black curve) in terms of peak positions and profiles.
102 The simulations were performed in 3D and the geometry followed the real sample. An
103 oblique incidence with an angle 57° was used to mimic the dark field illumination.

104 Five nanospheres with size difference from 20 nm down to single digit nm are
105 selected for spectral characterization (Fig. 2(a)). The diameter of each nanosphere is
106 obtained through SEM inspection of the same particle at a high magnification. In
107 order to reduce the influence of the stray-light transmission peak from the thin Au
108 film itself, the spectrum measured at a blank area is subtracted as a background from
109 that measured at each nanosphere (Fig. 2(b)). For example, the curve for nanosphere
110 No. 5 is obtained by subtracting the blue curve from the black curve in Fig. 1(e), thus
111 revealing the main peak associated with the resonance of the metal-dressed SiO₂
112 nanosphere. With the sphere size increasing from 421 nm to 486 nm, this peak is
113 red-shifted accordingly as confirmed by simulations (red dashed curves). It is worth
114 noting that a size difference as small as 8 nm between nanosphere No. 1 and 2 could
115 be clearly identified by the peak shift in spectrum, while they appear the same without
116 the metal dressing. Since the Mie resonance is within the visible range, the peak shift
117 due to size variation could also be distinguished by the color difference. As this
118 resonance is red-shifted with the increasing sphere size, the color of the nanospheres
119 in the dark field transmission view varies from green to orange (Fig. 2(c)). By
120 calibrating colors with spectra, sizes of nanospheres could be read out directly
121 through their colors with some accuracy [19]. In comparison, the SEM image (Fig.
122 2(d)) with the same field of view and the same magnification of the optical
123 microscope image (Fig. 2(c)) fails to tell the size difference; only zoom-in to
124 individual particles can tell its exact size. In addition, the enhanced Mie resonance is

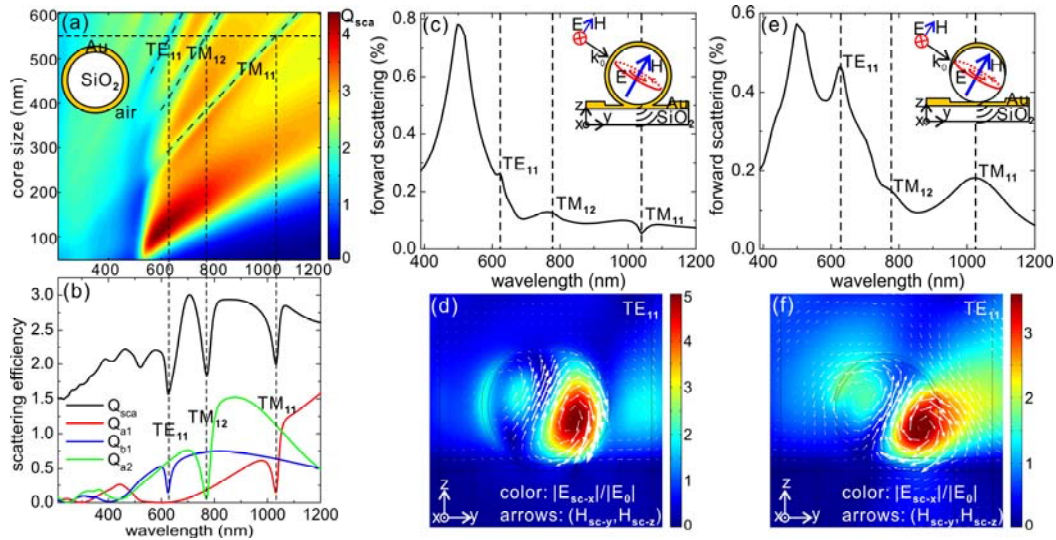
125 robust against small variations in the metal dressing. A 5 nm deviation in the thickness
 126 of each metal deposition step does not affect the resonant frequency [19].



127
 128 Fig. 2 (a) SEM images of five selected metal-dressed SiO₂ nanospheres with different
 129 sizes. (b) Background subtracted forward scattering spectra (black lines) of the five
 130 nanospheres and the corresponding simulations (dashed red lines). (c) Photopicture in
 131 the dark field transmission view for nanospheres including the five selected ones with
 132 size dependent colors. (d) SEM image of the same nanospheres in (c) with the same
 133 scope and the same magnification.

134 The pronounced peak in the forward scattering spectra is revealed as an
 135 enhanced Mie resonance by comparing the metal-dressed SiO₂ nanospheres with
 136 complete-metal-shell ones. Fig. 3(a) presents the scattering efficiency Q_{sc} of a
 137 complete-Au-shell SiO₂ nanosphere in air as a function of wavelength and core size
 138 based on Mie theory [1,24]. The shell thickness remains 30 nm.

139 $Q_{sc} = \frac{2}{(k_0 r)^2} \sum_{n=1}^{\infty} (2n+1) (|a_n|^2 + |b_n|^2)$, where k_0 is free space wave vector; r is the core
140 radius; a_n and b_n are coefficients of the scattered field decomposed in the basis of
141 vector spherical harmonics [1,24]. Due to the tight light confinement provided by the
142 metal shell, the Mie resonances of the SiO₂ nanosphere are significantly enhanced but
143 become less radiant at the same time. Through interaction, the Mie resonances show
144 up as Fano dips (cutting lines in Fig. 3(a)) in the background of the metal sphere
145 scattering [25,26], leading to resonant scattering suppression. Fig. 3 (b) shows Q_{sc} at
146 the core size of 550 nm and the decomposed contributions from the first three
147 fundamental Mie modes: $Q_{a_1} = 6|a_1|^2 / (k_0 r)^2$, $Q_{b_1} = 6|b_1|^2 / (k_0 r)^2$ and
148 $Q_{a_2} = 10|a_2|^2 / (k_0 r)^2$. a_1 , b_1 and a_2 correspond to the TM₁₁, TE₁₁ and TM₁₂ mode,
149 respectively. TM/TE stands for transvers magnetic/electric modes with no radial
150 magnetic/electric field. The subscripts denote different orders. For a better
151 comparison with our experiment, the complete-Au-shell nanosphere is located on a
152 Au film and illuminated under dark field scheme (Fig. 3(c) inset). The Au film has a
153 30 nm indentation below the nanosphere and is 60 nm thick elsewhere. The shell
154 merges with the Au plane at the bottom. As shown in Fig. 3(c), the Mie resonances are
155 observed in the simulated forward scattering spectrum at the same wavelengths as
156 those in Fig. 3(a) and (b). In this case, the three resonances are still less radiant and
157 thus show Fano shapes in the background of the transmission through the Au film.
158 The light field distribution at the TE₁₁ resonance (Fig. 3(d)) reveals the mode pattern
159 as a an inclining magnetic dipole (MD) with electric field vortex circulating around it,
160 as diagrammatically sketched by the inset of Fig. 3(c).



161

162 Fig. 3 (a) Scattering efficiency (Q_{sca}) spectrum at different core sizes of the
 163 complete-shell nanosphere (shell thickness 30 nm) in air. (b) Q_{sca} spectrum at the core
 164 size of 550 nm (indicated by the horizontal dashed line in (a)) and the decomposed
 165 contributions from the first three fundamental Mie modes (TM_{11} , TE_{11} and TM_{12}). (c)
 166 Forward scattering spectrum of the complete-shell nanosphere (core size 550 nm)
 167 located on a Au film under dark field illumination. (d) Distributions of scattered
 168 electric field x -component $|E_{sc-x}|$ and scattered in-plane magnetic field vector (H_{sc-y} ,
 169 H_{sc-z}) at the TE_{11} resonance on the y - z plane at $x=0$. (e) and (f) Forward scattering
 170 spectrum and field distribution of the metal-dressed nanosphere (486 nm) at the TE_{11}
 171 resonance.

172 Fig. 3(e) presents the simulated forward scattering spectrum of a metal-dressed SiO_2
 173 nanosphere with a diameter around 486 nm. This spectrum is the same as the dashed
 174 red line in Fig. 1 (e) but extended to longer wavelengths. Fig. 3(f) presents the field
 175 distribution at the resonance (~ 630 nm). A direct comparison between Fig. 3(d) and (f)
 176 reveals that the pronounced peak we observed in experiment corresponds to the
 177 enhanced TE_{11} Mie resonance of the SiO_2 nanosphere. In another model, the enhanced
 178 TE_{11} Mie mode could be considered as a Fabry-Perot (F-P) resonance of a waveguide
 179 mode propagating at a tilted angle (Fig. 3 (f)). Compared to the mode pattern of the
 180 metal-sandwiched cylindrical waveguide, the light field inside the metal-dressed
 181 sphere could be regarded as a standing wave of the waveguide mode due to multiple
 182 reflections [19]. The waveguide mode F-P resonance in our configuration is a
 183 localized mode confined in the metal-dressed nanoparticle, and therefore insensitive

184 to the incident angle. Although a complete metal shell provides a better light
185 confinement than the metal dress as revealed by the higher field concentration inside
186 the SiO₂ nanosphere (comparison between Fig. 3(d) and (e)), the metal dress is much
187 more favorable to fabrication. Core-shell structures below 100 nm could be created by
188 chemical synthesis [27]. However, making larger shells (several hundred nm to 1 μm)
189 is much tougher than making a metal dress by a two-step deposition. Further, the Mie
190 resonances in the metal-dressed nanosphere appear as peaks in scattering spectra (Fig.
191 1(e) and Fig. 3(e)), while the Mie resonances in the complete-shell nanosphere appear
192 as Fano dips (Fig. 3(a)-(c)). The metal dress not only enhances the Mie resonances by
193 providing high reflecting boundaries but also couples the Mie mode into the far field
194 by serving as an antenna.

195 The enhanced TE₁₁ Mie resonance is associated with a MD resonance since the
196 field distribution (Fig. 3(f)) shows circulating displacement currents and an intensified
197 magnetic field at the center. Actually, the ideal TE₁₁ Mie resonance of a nanosphere
198 could just be regarded as a MD resonance [1]. The magnetic response of high-index
199 dielectric nanoparticles is mainly due to that and have attracted much attention
200 [7,8,12]. Since the circulating displacement current density ($J_D = (-i\omega)\epsilon_0\epsilon_r E$) as well
201 as the induced MD increases with permittivity, prominent magnetic responses are
202 observed. From another point of view, one need not to rely solely on the high
203 refractive index to produce strong magnetic resonances if a strong *E*-field can be
204 obtained [12]. Typically intensified *E*-field can be obtained in an optical cavity with
205 high Q-factor modes. Since low-index particles provide very weak light confinement
206 and therefore low-Q Mie modes, they are typically are not suited for inducing
207 magnetic response. However, with help of the metal dressing, the Mie modes of
208 low-index nanoparticles are greatly enhanced. At the TE₁₁ mode (Fig. 3(f)), the strong
209 circulating electric field leads to strong circulating displacement currents and thus a
210 strong MD. This result implies that considerable magnetic response could also be
211 induced in low-index nanoparticles by a simple metal dressing process. Nevertheless,
212 due to the induced currents in the metal dress, the optical response at the TE₁₁ Mie

213 resonance is not a pure MD response. Other components could be identified by a
214 multipole decomposition calculation based on the simulated light field distributions
215 [19]. In the view of method of images, the tilted MD on a Au film could be considered
216 as the MD with its image and the appearance of high order multipoles is reasonable
217 [19].

218 The enhanced Mie resonance is distinguished from plasmon modes. The Mie
219 mode is concentrated within the SiO₂ nanosphere as an optical cavity while plasmon
220 modes are typically at metal/dielectric interfaces [19]. Moreover, the Mie mode is also
221 different from split ring like resonances, associated with highly concentrated field
222 within the split gaps [28], although the metal dress shares some similarities with a
223 split shell. The metal dressing process has also been applied to semiconductor
224 nanorods with high refractive index for plasmonic cloaking [29,30] and nanoscale
225 color filtering [31]. For deep-subwavelength sizes, when the induced electric dipole
226 moment in the core and that in the shell are equal in magnitude but opposite in sign,
227 scattering cancellation is realized. For spheres with larger sizes in our case, phase
228 retardation plays a role and Mie modes become the key factor of scattering properties.

229 The enhanced Mie resonances as local modes could be utilized for sensing the
230 individual low-index nanospheres. Low-index nanoparticles such as SiO₂ and
231 polystyrene nanospheres have a wide range of important applications [32-38]. Sensing
232 the local properties of individual nanoparticles, such as size and refractive index, in a
233 proper manner would greatly benefit all those applications. The enhanced Mie
234 resonances as peaks in scattering spectra could work for sensing. Since the resonance
235 occurs in the visible range, the minute size difference could also be sensed by color
236 difference. After mapping the particle size with color, we could obtain the sizes of all
237 the nanospheres in one micrograph by analyzing their colors. Compared to SEM
238 inspection and dynamic light scattering, this colorimetric approach could lead to a
239 new particle sizing method with both efficiency and accuracy [19]. When particle size
240 is fixed, a minute change in refractive index of the particle could be sensed by shift of
241 the enhanced Mie resonance [19].

242 In summary, the metal dress created by a two-step deposition process

243 prominently enhances the Mie resonances of low-index nanoparticles. The metal dress
244 improves light confinement ability of low-index nanoparticles by enhancing boundary
245 reflection and thus enhances the Mie resonances. Beyond a high reflection cavity, the
246 metal dress also functions as a broadband antenna to couple the concentrated light
247 power to the far field. The resonance occurring in the visible range leads to size
248 dependent colors. At the enhanced TE_{11} Mie resonance, the intensified E -field instead
249 of high permittivity induces strong circulating displacement currents and thus
250 considerable magnetic response. The enhanced Mie resonances could be used to sense
251 minute changes in size or refractive index of low-index nanoparticles and benefit
252 many applications.

253

254 ACKNOWLEDGMENT

255 The authors appreciate the discussion with You-chia Chang about the spectrum
256 measurement of a single nanoparticle. This work is supported in part by the NSF grant
257 DMR 1120923; J.Z. acknowledges the support by the Hundred Talent Program of the
258 Chinese Academy of Sciences, the National Natural Science Foundation of China
259 grant No. 61605230, the Shanghai Pujiang Program 16PJ1410400 and the National
260 Key Research and Development Program of China grant No. 2017YFA0205801.

261

262 REFERENCES:

- 263 [1] C. F. Bohren, D. R. Huffman, Absorption and Scattering of Light by Small
264 Particles. New York: Wiley, 1983.
- 265 [2] K. L. Kelly, E. Coronado, L. L. Zhao, G. C. Schatz, The optical properties of
266 metal nanoparticles: The influence of size, shape, and dielectric environment. *J.*
267 *Phys. Chem. B* **107**, 668–677 (2003).
- 268 [3] K.-S. Lee, M. A. El-Sayed, Gold and Silver Nanoparticles in Sensing and
269 Imaging: Sensitivity of Plasmon Response to Size, Shape, and Metal
270 Composition, *J. Phys. Chem. B* **110**, 19220-19225 (2006).
- 271 [4] J. N. Anker, W. P. Hall, O. Lyandres, N. C. Shah, J. Zhao, R. P. Van Duyne,
272 Biosensing with plasmonic nanosensors. *Nat. Mater.* **7**, 442-453 (2008).

- 273 [5] A. I. Kuznetsov, A. E. Miroshnichenko, M. L. Brongersma, Y. S. Kivshar, B.
274 Luk'yanchuk, Optically resonant dielectric nanostructures. *Science* **354**, aag2472
275 (2016).
- 276 [6] J. C. Ginn, I. Brener, Realizing optical magnetism from dielectric metamaterials.
277 *Phys. Rev. Lett.* **108**, 097402 (2012).
- 278 [7] L. Shi, T. U. Tuzer, R. Fenollosa, F. Meseguer, A New Dielectric Metamaterial
279 Building Block with a Strong Magnetic Response in the Sub-1.5-Micrometer
280 Region: Silicon Colloid Nanocavities. *Adv. Mater.* **24**, 5934–5938 (2012).
- 281 [8] A. B. Evlyukhin, S. M. Novikov, U. Zywietz, R. L. Eriksen, C. Reinhardt, S. I.
282 Bozhevolnyi, B. N. Chichkov, Demonstration of magnetic dipole resonances of
283 dielectric nanospheres in the visible region. *Nano Lett.* **12**, 3749–3755 (2012).
- 284 [9] S. Nie, S. R. Emory, Probing Single Molecules and Single Nanoparticles by
285 Surface-Enhanced Raman Scattering, *Science* **275**, 1102 (1997).
- 286 [10] S. Lal, S. Link, N. J. Halas, Nano-optics from sensing to waveguiding, *Nat.*
287 *Photonics.* **1**, 641 (2007).
- 288 [11] J. A. Fan, C. Wu, K. Bao, J. Bao, R. Bardhan, N. J. Halas, V. N. Manoharan, P.
289 Nordlander, G. Shvets, F. Capasso, Self-Assembled Plasmonic Nanoparticle
290 Clusters **328**, 1135 (2010).
- 291 [12] B.-I. Popa, S. A. Cummer, Compact dielectric particles as a building block for
292 low-loss magnetic metamaterials. *Phys. Rev. Lett.* **100**, 207401 (2008).
- 293 [13] Y. H. Fu, A. I. Kuznetsov, A. E. Miroshnichenko, Y. F. Yu, B. Luk'yanchuk,
294 Directional visible light scattering by silicon nanoparticles. *Nat. Commun.* **4**,
295 1527 (2013).
- 296 [14] S. Zhang, R. Jiang, Y.-M. Xie, Q. Ruan, B. Yang, J. Wang, H.-Q. Lin,
297 Moderate-Refractive-Index Cu₂O Nanospheres as Visible-Region Nanoantennas
298 with Electromagnetic Resonance and Directional Light-Scattering Properties. *Adv.*
299 *Mater.* **27**, 7432–7439 (2015).
- 300 [15] S. Person, M. Jain, Z. Lapin, J. J. Sáenz, G. Wicks, L. Novotny, Demonstration of
301 zero optical backscattering from single nanoparticles. *Nano Lett.* **13**, 1806–1809
302 (2013).

- 303 [16] A. E. Miroshnichenko, A. B. Evlyukhin, Y. F. Yu, R. M. Bakker, A. Chipouline, A.
304 I. Kuznetsov, B. Luk'yanchuk, B. N. Chichkov, Y. S. Kivshar, Nonradiating
305 anapole modes in dielectric nanoparticles, *Nat. Commun.* **6**, 8069 (2015).
- 306 [17] M. Cortie, M. Ford, A plasmon-induced current loop in gold semi-shells,
307 *Nanotechnology* **18**, 235704 (2007).
- 308 [18] J. B. Lassiter, M. W. Knight, N. A. Mirin, N. J. Halas, Reshaping the Plasmonic
309 Properties of an Individual Nanoparticle, *Nano Lett.* **9**, 4326 (2009).
- 310 [19] See Supplemental Material at [URL will be inserted by publisher] for the
311 influence of the metal thickness on the enhanced resonance; optical responses of
312 uncoated SiO₂ nanospheres and the shallow nano wells; further comparison
313 between the complete-shell SiO₂ nanosphere and the metal-dressed SiO₂
314 nanosphere; analysis based on the method of images; modelling by waveguide
315 mode F-P resonances; angle dependence of the enhanced resonance; plasmon
316 modes of the metal dress; particle sizing by the colorimetric method; and index
317 sensing based on the enhanced resonance, which includes Refs. [20-23].
- 318 [20] I. Staude, A. E. Miroshnichenko, M. Decker, N. T. Fofang, S. Liu, E. Gonzales, J.
319 Dominguez, T. S. Luk, D. N. Neshev, I. Brener, Y. Kivshar, Tailoring Directional
320 Scattering through Magnetic and Electric Resonances in Subwavelength Silicon
321 Nanodisks, *ACS Nano* **7**, 7824 (2013).
- 322 [21] J. van de Groep, A. Polman, Designing dielectric resonators on substrates:
323 Combining magnetic and electric resonances, *Opt. Express* **21**, 26285 (2013).
- 324 [22] M. Decker, I. Staude, M. Falkner, J. Dominguez, D. N. Neshev, I. Brener, T.
325 Pertsch, Y. S. Kivshar, High-Efficiency Dielectric Huygens' Surfaces, *Adv. Opt.*
326 *Mater.* **3**, 813 (2015).
- 327 [23] Y. Yamaguchi, Y. Yamada, J. Ishii, *Int. J. Thermophys.* **36**, 1825–1833 (2015).
- 328 [24] C. Mätzler, MATLAB Functions for Mie Scattering and Absorption, Institut für
329 Angewandte Physik, Research Report No. 2002-08, Bern, Switzerland, 2002.
- 330 [25] W. Chaabani, A. Chehaidar, J. Plain, Comparative Theoretical Study of the
331 Optical Properties of Silicon/Gold, Silica/Gold Core/Shell and Gold Spherical
332 Nanoparticles, *Plasmonics* **11**, 1525–1535 (2016).

- 333 [26]J. S. Parramon, D. Jelovina, Boosting Fano resonances in single layered.
334 Nanoscale **6**, 13555 (2014).
- 335 [27]S. J. Oldenburg, R. D. Averitt, S. L. Westcott, N. J. Halas, Nanoengineering of
336 optical resonances, Chem. Phys. Lett. **288**, 243–247 (1998).
- 337 [28]A. I. Kuznetsov, A. E. Miroschnichenko, Y. H. Fu, V. Viswanathan, M. Rahmani,
338 V. Valuckas, Z. Y. Pan, Y. Kivshar, D. S. Pickard, B. Luk'yanchuk, Split-ball
339 resonator as a three-dimensional analogue of planar split-rings. Nat. Commun. **5**,
340 3104 (2014).
- 341 [29]P. Fan, U. K. Chettiar, L. Cao, F. Afshinmanesh, N. Engheta, M. L. Brongersma,
342 An invisible metal–semiconductor photodetector. Nat Photon. **6**, 380-385 (2012).
- 343 [30]A. Alù, N. Engheta, Achieving transparency with plasmonic and metamaterial
344 coatings. Phys. Rev. E **72**, 016623 (2005).
- 345 [31]J. K. Hyun, T. Kang, H. Baek, D.-s. Kim, G.-c. Yi, Nanoscale single-element
346 color filters. Nano Lett. **15**, 5938–5943 (2015).
- 347 [32]C. L. Haynes, R. P. Van Duyne, Nanosphere lithography: a versatile
348 nanofabrication tool for studies of size-dependent nanoparticle optics. J. Phys.
349 Chem. B **105**, 5599-5611 (2001).
- 350 [33]I. I. Slowing, B. G. Trewyn, S. Giri, V. S.-Y. Lin, Mesoporous silica nanoparticles
351 for drug delivery and biosensing applications. Adv. Funct. Mater. **17**, 1225-1236
352 (2007).
- 353 [34]M. Liong, J. Lu, M. Kovichich, T. Xia, S. G. Ruehm, A. E. Nel, F. Tamanoi, J. I.
354 Zink, Multifunctional inorganic nanoparticles for imaging, targeting, and drug
355 delivery. ACS Nano **2**, 889-896 (2008).
- 356 [35]M. De, P. S. Ghosh, V. M. Rotello, Applications of nanoparticles in biology. Adv.
357 Mater. **20**, 4225-4241 (2008).
- 358 [36]J. Kim, H. S. Kim, N. Lee, T. Kim, H. Kim, T. Yu, I. C. Song, W. K. Moon, T.
359 Hyeon, Multifunctional Uniform Nanoparticles Composed of a Magnetite
360 Nanocrystal Core and a Mesoporous Silica Shell for Magnetic Resonance and
361 Fluorescence Imaging and for Drug Delivery. Angew. Chem. Int. Ed. **47**,
362 8438-8441 (2008).

- 363 [37]J. Bravo, L. Zhai, Z. Wu, R. E. Cohen, M. F. Rubner, Transparent
364 superhydrophobic films based on silica nanoparticles. *Langmuir* **23**, 7293-7298
365 (2007).
- 366 [38]M. Manca, A. Cannavale, L. De Marco, A. S. Arico, R. Cingolani, G. Gigli,
367 Durable superhydrophobic and antireflective surfaces by trimethylsilanized silica
368 nanoparticles-based sol-gel processing. *Langmuir* **25**, 6357–6362 (2009).